AIAA JOURNAL
Vol. 42, No. 1, January 2004

Postbuckling Behavior of Segmented Circular Composite Cylinders

Jaret C. Riddick*
U.S. Army Research Laboratory, Hampton, Virginia 23681
and
Michael W. Hyer†
Virginia Polytechnic Institute and State University, Blacksburg, Virginia 24061

The response characteristics of composite cylinders constructed in four circumferential segments are discussed. Two cylinder configurations, referred to as axially stiff and circumferentially stiff cylinders, are studied. Numerical results from STAGS finite element analyses are presented and include predicted radial displacements and selected stress resultants. Compressive loading into the postbuckling range by an axial endshortening is considered. The results show that, as the endshortening increases toward the buckling value, some segments of the cylinders begin to develop axial wrinkles, whereas other segments remain relatively unwrinkled. For the two cylinders considered here, the wrinkling of the segments is correlated with the level of axial stress resultant supported in the segment. Load drops of 20 and 57% for the axially stiff and circumferentially stiff cylinders, respectively, are predicted for levels of endshortening beyond the buckling values. The postbuckled cylinders are characterized by regions of large localized inward dimples and outward ridges in the radial displacement pattern. These regions are sites of large-magnitude axial and transverse shear stress resultants.

Introduction

In the future, composite fuselage structures may well be made in such a way that the laminate stacking sequence varies with circumferential location around the fuselage. The stacking sequence at the top and bottom of the fuselage may be axially stiff to resist axial tensile and compressive loads due to fuselage bending, whereas the sides may be designed to resist shear loading. Figure 1 illustrates a section of a fuselage idealized as a circular cylinder, with the crown, side, and keel constructed of different laminates. Though the subtended angle for the crown and keel do not have to be the same, here they are assumed to each subtend the angle $2\theta^*$. As a result of the discrete change in stiffness in the circumferential direction, the response of the cylinder to even simple axisymmetric loadings such as axial compression or internal pressure could result in axial, circumferential, and radial displacements that are not uniform with respect to circumferential location. The resulting displacement gradients in the circumferential direction could, in turn, lead to unfavorable stress fields where the segments join. Additionally, the variation in stiffness and the nonuniform stresses could influence buckling and postbuckling behavior. Therefore, one objective of the present work is to obtain an understanding of the influence of segmented construction on overall cylinder response, particularly in the postbuckling range of axial compression. This objective is met by developing finite element models and studying the predicted results.

The behavior of any size segmented composite cylinder subjected to a variety of loads can be studied using finite elements. However, to conduct experiments, due to fabrication and fixturing costs and facilities requirements, small-scale cylinders are better for initial studies than fuselage-size cylinders. The downside is that the method of fabrication can have more of an effect on small-scale cylinders than on large-scale cylinders, as can the method of load introduction. As part of this study, two small-scale graphite–epoxy segmented cylinders have been constructed, and there are plans to record their behavior when loaded in axial compression by way of axial endshortening. Therefore, a second objective of the present study is to obtain an understanding of the response of these two particular cylinders both to know what to expect and so the placement of displacement transducers, strain gauges, and other instrumentation in the test setup can be done judiciously. The use of a finite element model also meets this objective because details of how these particular cylinders are fabricated and the method of load introduction during the tests are included in the model.

Research on the response of cylinders has been ongoing for decades and has resulted in references too numerous to discuss. A search of databases will list thousands of citations. Narrowing the search by specifying interest in the influence of boundary conditions, or imperfections, or shear deformations, or higher-order effects will still result in hundreds of citations. However, many of the more recent studies take advantage of modern day finite element analyses that can account for geometric nonlinearities, bifurcated solutions, instabilities, and transient dynamic analyses and can be categorized as high-fidelity analysis tools.[1] Such tools have been used to study, in fine detail, the role of imperfections in materials and geometry,[2] mode jumping,[3] the role of discontinuities, such as cutouts,[4] and even progressive failure.[5] The work described here fits into this category of analysis and utilizes the finite element structural analysis of general shells code STAGS[6] to study in detail a particular problem of importance. Additionally, there does not appear to be any previous efforts on the problem addressed.

In the next section, some of the details of the construction of two specific small-scale cylinders that have been fabricated are discussed, and the finite element model of these cylinders is described. The finite element model is used to predict the response of these two cylinders from low levels of axial endshortening to postbuckling levels. In this work, the response is characterized by examining the radial displacements and selected stress resultants. Though there are many aspects of cylinder response, a discussion of these variables conveys some of the interesting features.

Presented as Paper 2001-1397 at the AIAA 42nd Structures, Structural Dynamics, and Materials Conference, Seattle, WA, 16–19 April 2001; received 18 June 2002; accepted for publication 4 August 2003.

*Aerospace Engineer, NASA Langley Research Center, Mail Stop 188B; j.c.riddick@larc.nasa.gov.

†Professor, Department of Engineering Science and Mechanics (0219); hyerm@vt.edu. Associate Fellow AIAA.

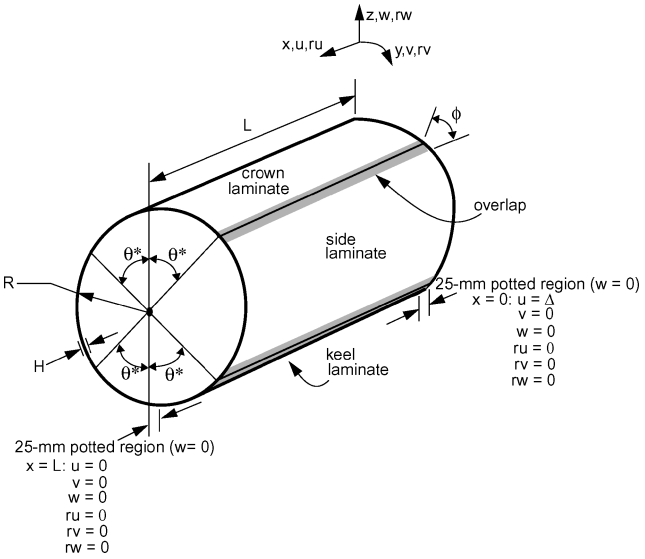

Fig. 1 Geometry and nomenclature for analysis of segmented cylinders.

Fig. 2 Photograph of the axially stiff specimen.

Cylinders Details and Modeling

Two cylindrical specimens with inner diameters of 0.254 m (10 in.) and lengths of 0.432 m (17 in.) were fabricated using 0.305-m (12.0-in.)-wide unidirectional Hercules AS4/3501-6 graphite–epoxy prepreg tape 0.1397 mm (0.0055 in.) thick. The angle $2\theta^*$, which was measured to the centers of the overlaps, was 60 deg. An aluminum mandrel was used to form the cylinders. The cylinders had eight-layer segments and were configured as follows: For the axially stiff cylinder, the lamination sequence was $[\pm 45/0_2]_S$ for the crown and keel and $[\pm 45]_{2S}$ for the sides, where 0 deg corresponds to the axial direction of the cylinder. For the circumferentially stiff cylinder, the lamination sequence was $[\pm 45/90_2]_S$ for the crown and keel, and the side laminates were the same as for the axially stiff cylinder. The direction of the greater stiffness in the crown and keel segments reflect the nomenclature used to identify the two cylinders. Adjacent segments were joined by splicing, or overlapping, the plys. Each overlap spanned the circumferential angle ϕ, shown as the shaded region in Fig. 1. The overlap segments were constructed to be symmetric 12-layer laminates. For the axially stiff case, the overlap lamination sequence was $[\pm 45/0/+45/0/-45]_S$, whereas for the circumferentially stiff case the overlap lamination sequence was $[\pm 45/90/+45/90/-45]_S$. The overlaps were 12.70 mm (0.5 in.) in the circumferential dimension. As a result of the thickness of a single layer being 0.1397 mm (0.0055 in.), the thickness of the crown, keel, and sides was 1.118 mm (0.044 in.) and that of the overlaps 1.676 mm (0.066 in.).

It is important to realize that manufacturing a small-scale circular segmented cylinder on a mandrel has an influence on the details of the overlap region. Specifically, though the overlap has a greater number of plies than the adjoining segments, and is therefore thicker, the inner radii of the four segments and the four overlap regions are the same. This occurs because the cylinder is fabricated from the outer surface of the mandrel outward. As a result, there is a radial offset, or eccentricity, between the midsurface of the thicker laminates, which constitute the overlaps, and the midsurfaces of the laminates making up the adjacent segments. In particular, the radial offset, or eccentricity, of the overlap was two layer thicknesses, or 0.279 mm (0.011 in.). The eccentricity of the overlap regions had an influence on the overall response.

The cylinders were cured in an autoclave and used a vacuum bag to ensure good cohesion between the plys. Because of imperfections at the cylinder ends due to the vacuum port in the vacuum bag, the lengths of the cylinders were trimmed. The cylinder ends were potted in an aluminum-filled epoxy and steel band arrangement to prevent premature failure of the cylinder ends due to brooming and to enforce clamped end conditions. The potted ends were then machined flat and parallel to mate with the flat loading platens of the load frame used to apply the compressive endshortening. The final cylinder length was 0.356 m (14 in.). A photograph of the axially stiff cylinder is shown in Fig. 2. The keel, an overlap, and a side are visible, and the potted ends can be seen.

The finite element models were developed using the STAGS finite element program. The STAGS 410 quadrilateral shell element was used. There were 57 elements in the axial direction in each segment. In the circumferential direction, the crown and keel each had 12 elements, the sides 30 elements, and the overlaps 5 elements each, for a total of 104 elements in the circumferential direction. Other mesh densities were investigated to study convergence, and this particular mesh provided answers that compared well with the others. Numerical results from this mesh are presented here. Referring to Fig. 1, x is the axial coordinate, as measured from one end, u is the axial displacement, y is the circumferential arclength coordinate, as measured from the center of the crown, v is the circumferential displacement, and w is the radial displacement, measured positive outward. The mean radius of the cylinder is R, the length L, and the thickness of the crown, keel, and side segments H. Because the epoxy and steel band potting arrangement on each end encompassed 25.4 mm (1 in.) of axial length, the unsupported cylinder length is 0.305 m (12 in.). The full 0.356 m (14 in.) length is modeled with finite elements, with 25.4 mm (1 in.) on each end devoted to simulate the effects of the potting by enforcing the condition of no radial displacement in the potted region. The end at $x = L$ is further restrained from axial and circumferential movements and any rotations, denoted as ru, rv, and rw in STAGS. The end at $x = 0$ is displaced a known amount Δ in the $+x$ direction to develop the compressive endshortening, but restrained from circumferential motion and rotations. These boundary conditions are shown in Fig. 1. It is assumed that all material properties are linear elastic, and the engineering properties of a single layer of material are assumed to be

$$E_1 = 130.0 \text{ GPa}, \qquad E_2 = 9.70 \text{ GPa}$$
$$G_{12} = 5.00 \text{ GPa}, \qquad \upsilon_{12} = 0.300 \tag{1}$$

Geometric nonlinearities are included in all calculations.

With the finite element analysis, axial endshortening is applied, starting from zero, increasing through what could be considered the geometrically linear prebuckling range of response, through the geometrically nonlinear prebuckling range of response, to buckling, and finally into the postbuckling, or collapse, range.

Predicted Response

The responses of the two cylinders in the various ranges of compressive endshortening are quite interesting. To focus the discussion of the responses, the various ranges are denoted on the normalized load vs endshortening relations for the two cylinders, where the normalizing factors are the respective values at buckling, here denoted as P_{cr} and Δ_{cr}. There are a number of calculations that can be made to compute to so-called buckling conditions, and that will be discussed later. The normalized load vs endshortening relations for the two cylinders, as computed by the finite element analyses, are shown in Fig. 3. The linear and nonlinear prebuckling ranges, the buckling point, and the postbuckling range are identified. The dividing lines between the linear and nonlinear prebuckling ranges are somewhat subjective, but are shown to occur at about 50–60% of the buckling value. Knowing the exact dividing line is not critical because, as mentioned earlier, all analyses here include geometric nonlinearities. The response of both cylinders in Fig. 3 is characterized by a nearly linear increase in load with increasing endshortening almost to the buckling point, followed by a slightly nonlinear (softening) relation between load and endshortening to the buckling point, followed by a sudden decrease in load just after buckling. The load increases again with increasing endshortening in the postbuckling range. The actual values of P_{cr} and Δ_{cr} differ considerably for these two cases, so that relations not normalized and plotted on the same scale would look quite different than what Fig. 3 indicates. As points of reference, the value of P_{cr} for the axially stiff cylinder is 88,100 N (19,810 lb), whereas that for the circumferentially stiff cylinder is 142,500 N (32,000 lb). The values of Δ_{cr} are 0.891 and 2.76 mm (0.0351 and 0.1087 in.), respectively. The corresponding values of overall axial strain, Δ_{cr}/L, are $2500\mu\varepsilon$ and $7760\mu\varepsilon$, respectively. Note that the preceding values are all actually compressive.

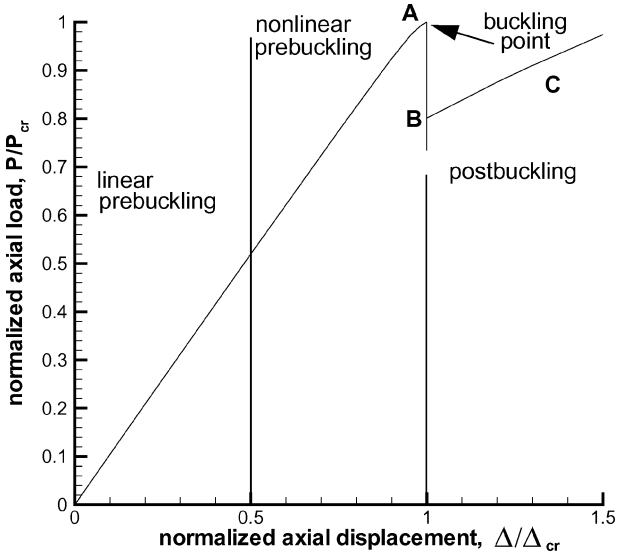

a) Axially stiff cylinder

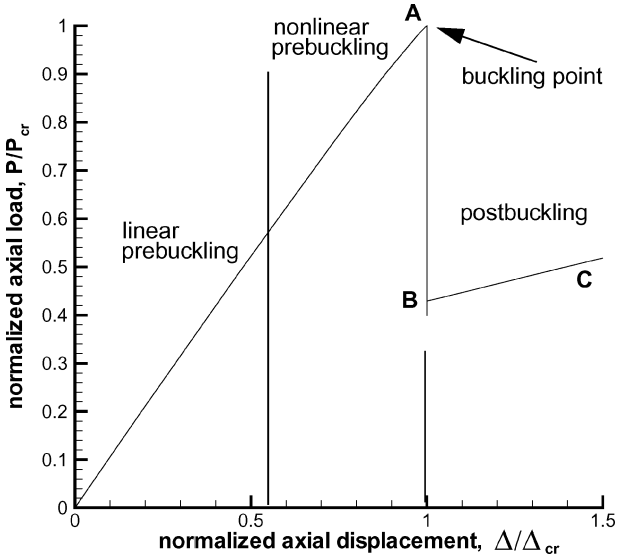

b) Circumferentially stiff cylinder

Fig. 3 Load vs endshortening response for segmented cylinders.

The discussion to follow is divided into four sections: linear prebuckling response, nonlinear prebuckling response, buckling response, and postbuckling response. Because the emphasis of this paper is on the postbuckling response, those details will be both discussed and shown. However, some aspects of the linear and nonlinear prebuckling response are quite interesting, and those will be described briefly. Including a description, though limited, of the prebuckling response provides a contrast for the postbuckling response. The computations for the linear prebuckling, nonlinear prebuckling, and buckling responses are carried out with a static finite element analysis. The postbuckling response is also computed with a static finite element analysis. However, the transition from the buckling point (point A of Fig. 3) to the initial point on the postbuckling path (point B) is computed with a transient dynamic finite element analysis. The transient analysis will be briefly described.

Linear Prebuckling Response

To study the response in the geometrically linear prebuckling range, an axial displacement is applied which produces an overall compressive axial strain of $1000\mu\varepsilon$. This condition corresponds to $\Delta/\Delta_{cr} = 0.399$ and $P/P_{cr} = 0.418$ for the axially stiff cylinder, whereas for the circumferentially stiff cylinder this condition corresponds to $\Delta/\Delta_{cr} = 0.1288$ and $P/P_{cr} = 0.1371$ (Fig. 3). The axial displacement response for both cylinders (not shown) is identical. The displacements vary linearly with the axial coordinate and are practically independent of the circumferential coordinate. This indicates that the axial displacement response is strictly a kinematic issue and does not depend on cylinder construction.

As is well known, a uniform cylinder constructed of a single symmetric balanced laminate and subjected to axial endshortening has no circumferential displacements. This is not the case for segmented construction because there are circumferential displacements for both cylinders. Basically, the two overlaps on both sides of the crown move toward the top of the crown, and the two overlaps on both sides of the keel move toward the bottom of the keel. The greatest circumferential displacement occurs at the cylinder midlength ($x = L/2$) at the overlap location. Geometrically linear studies conducted by Riddick and Hyer[7] indicate that the presence of circumferential displacements in segmented circular cylinders is due to a mismatch in Poisson's ratio between the crown, keel, and side segments, though the magnitude of the effect is controlled by the clamped boundary conditions.

The radial displacement response for both cylinders in the linear prebuckling range is shown in Figs. 4a and 4b. The displacement responses are shown as contour plots mapped onto the deformed finite element meshes. The displacements have been normalized by the segment thickness H, which corresponds to the eight-layer thickness of the crown, keel, and side laminates. The $w = 0$ condition in the potted regions (the dark band on each end) is quite obvious. For a cylinder of nonsegmented construction, that is, a cylinder constructed of a single laminate, subjected to axial endshortening, the radial displacement is characterized by an axisymmetric bending boundary-layer response near the ends of the cylinder that attenuates, depending on the cylinder length-to-radius ratio and material orthotropy, to a uniform or nearly uniform outward radial displacement away from the ends, the so-called membrane region. In contrast, for cylinders with segmented construction, there are boundary layers at the ends, but the radial displacement is generally not uniform away from the ends, so that there is no true membrane region. This is due to the variation of material properties with circumferential position. As can be seen from the contour plots (Figs. 4), at midlength the radial displacement varies with circumferential position. For the axially stiff cylinder, although the crown,

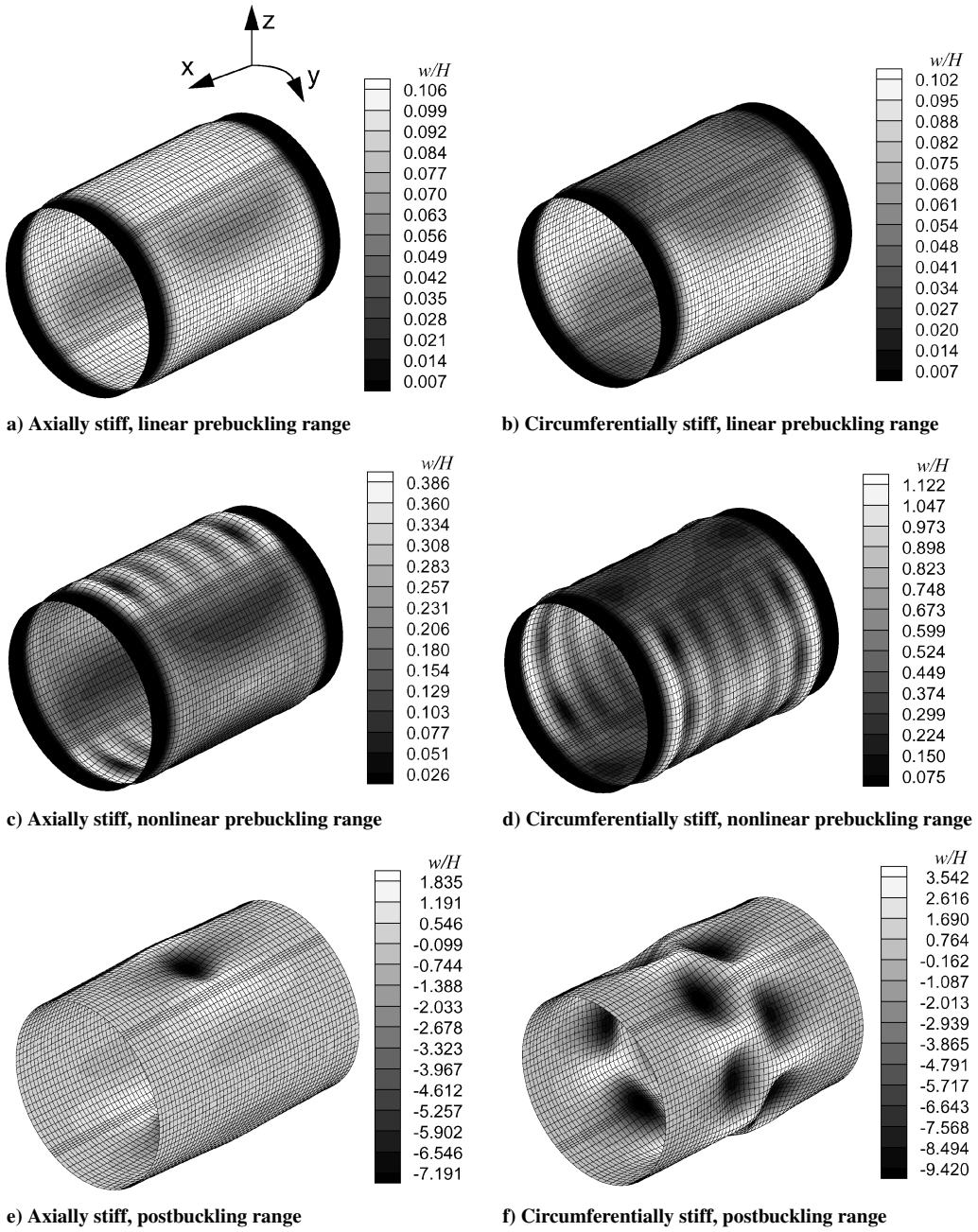

a) Axially stiff, linear prebuckling range

b) Circumferentially stiff, linear prebuckling range

c) Axially stiff, nonlinear prebuckling range

d) Circumferentially stiff, nonlinear prebuckling range

e) Axially stiff, postbuckling range

f) Circumferentially stiff, postbuckling range

Fig. 4 Normalized radial displacements, *w/H*.

keel, and sides have the same maximum radial displacements of $w/H \approx 0.1$, the radial displacement near the overlap regions in the side is less by about a factor of two, namely, $w/H \approx 0.06$. For the circumferentially stiff case, the maximum displacement in the crown and keel ($w/H \approx 0.06$) is about half of that in the sides ($w/H \approx 0.1$). The radial displacement variation with circumferential location can again be attributed to differences in Poisson's ratios and the clamped boundary conditions. Specifically, the outward radial displacement of an axially compressed circular cylinder constructed of a single laminate is directly proportional to the axial compressive strain and Poisson's ratio. With the crown, keel, sides, and overlaps each having different Poisson's ratios, there is a mismatch in radial displacement tendencies. These outward displacement tendencies are resisted by the clamped end conditions, and the degree to which the clamped end condition influences the radial displacements is a function of the axial bending stiffness. Because Poisson's ratio and the axial bending stiffness are different in the crown and keel as compared to the sides, a circumferentially varying displacement results, and the variation depends on axial location. Note, however, in both cases, for the linear prebuckling range the maximum displacements are only about 10% of the laminate thickness, a rather small displacement.

The compressive endshortening combined with the segmented construction produces an interesting variation of the stress resultants, that is, force and moment resultants, around the cylinder. The axial force resultant N_x for the axially stiff cylinder in the linear prebuckling range of loading is shown in Fig. 5a in the form of a contour plot. In Fig. 5a, the force resultant has been normalized by the average axial force resultant for the entire cylinder, so that the quantity shown is given by

$$\bar{N}_x = N_x/|P/2\pi R| \tag{2}$$

Note that the absolute value is used in the denominator, so that the sign of N_x is preserved. As can be seen, the overlap regions support the highest value of $N_x (\approx -2.0)$, the crown and keel the next highest value (≈ -1.9), and the sides the lowest value (≈ -0.6). Because the normalizing factor is the average value of N_x, it can be deduced that the overlaps and crown and keel support above average levels of N_x, whereas the sides support below average levels of N_x. In

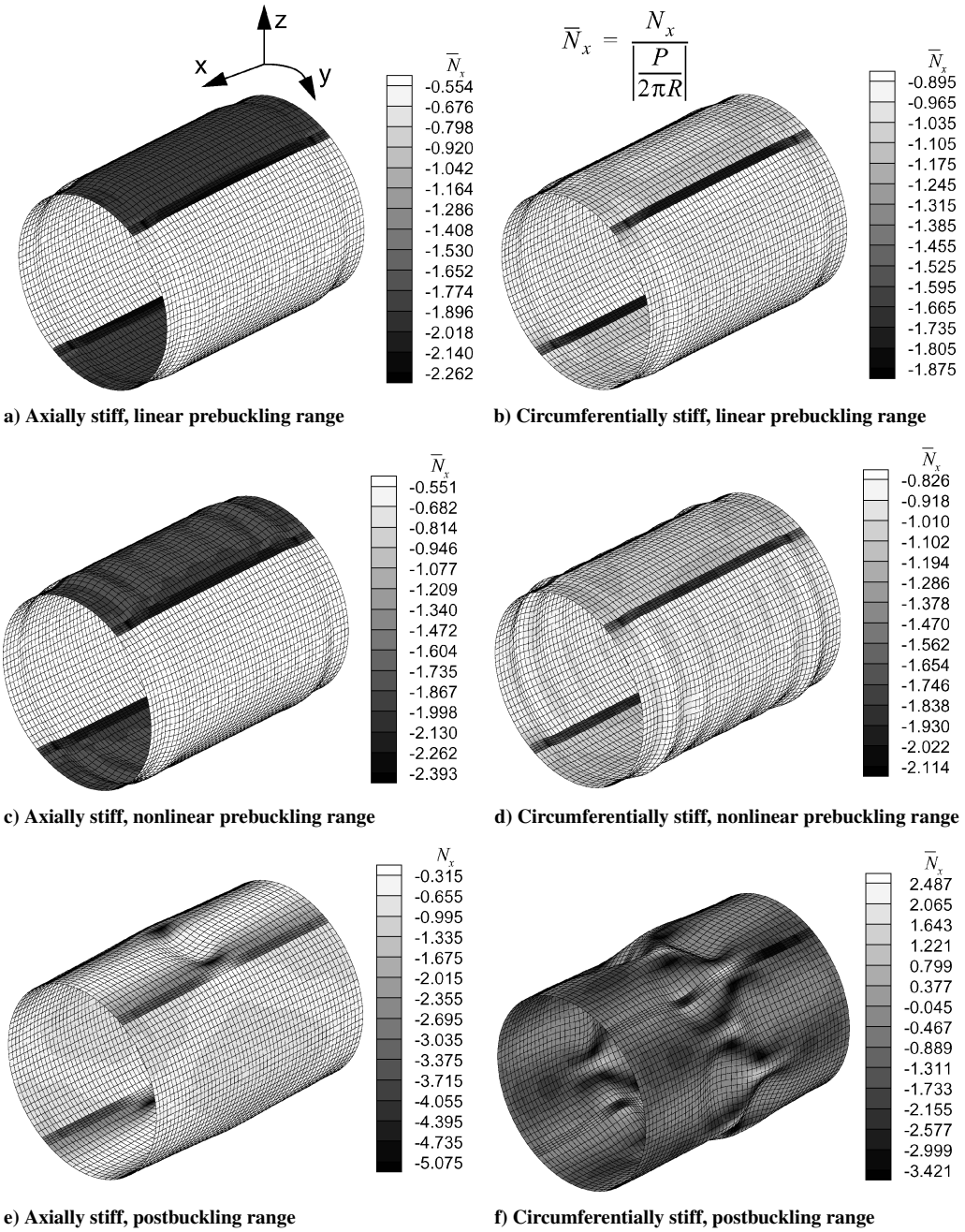

a) Axially stiff, linear prebuckling range

b) Circumferentially stiff, linear prebuckling range

c) Axially stiff, nonlinear prebuckling range

d) Circumferentially stiff, nonlinear prebuckling range

e) Axially stiff, postbuckling range

f) Circumferentially stiff, postbuckling range

Fig. 5 Normalized axial force resultant, $\bar{N}_x$.

particular, the crown and keel support about three times the level of N_x as the sides. Of course, the total load supported by a particular segment is the product of N_x and the circumferential arclength of the segment. If a particular segment supports above average loads, it might be expected to buckle before the other segments do. This also depends on the bending stiffness and arclengths involved. For the circumferentially stiff cylinder, the character of N_x is shown in Fig. 5b. Again, the overlap regions support the highest level of $N_x (\approx -1.8)$. The crown and keel also again support more than the sides (≈ -1.1 vs ≈ -0.9, respectively), but the difference in loading among the four segments is not as great as that exhibited by the axially stiff cylinder. Note that for both the axially stiff and circumferentially stiff cylinders, there are slight axial stress resultant concentrations in the overlaps at the cylinder ends caused by the clamped conditions there.

Note that the overlaps could be thought to be stiffeners for the cylinder. This is true only to a small degree. The overlaps are just 1.5 times as thick as the segments, and in the linear prebuckling range, they react only 2–4% of the total axial load. A true stiffener would be much thicker than the segments, and thus, react more of the axial load. Therefore, the overlaps are not a factor in controlling overall response, although they do add some interesting features to the response. However, if the segmented cylinder could be made by simply butting together the segments, instead of using overlaps, a significant portion of the cylinder response would be the same as with the overlaps.

The circumferential force resultant, referred to here as N_y (not shown), is practically zero except at the cylinder ends, where it is compressive due to the zero radial displacement condition there. The in-plane shear force resultant, referred to here as N_{xy}, is also close to zero everywhere, except in the overlap regions at the cylinder ends. Because of the aforementioned differences between Poisson's ratios and between other elastic properties of the segments and overlaps, at the overlaps there are mismatches in the what would be the kinematic responses of the segments if they were not part of the cylinder. These mismatches in kinematic response tendencies must be overcome by localized stress resultants to comply with the continuity conditions for displacements and slopes where the segments and overlaps join

and to comply with the kinematic boundary conditions at the ends of the cylinder. In the linear prebuckling range of endshortening, these continuity and boundary conditions result in stress resultant concentrations for N_{xy} at the cylinder ends in the overlap regions. This was also seen to some degree in Figs. 5a and 5b for N_x.

The magnitude of the axial transverse shear force resultant, referred to here as Q_x, is directly related to the level of interlaminar shear stress within the cylinders walls. High levels of Q_x could be associated with interlaminar failure. In the linear prebuckling range, the value of Q_x is zero in all of the cylinder except near the cylinder ends. There is a nonzero value of Q_x near the ends as a result of requiring w to be zero there. Because the overlap regions are stiffer in bending than the crown, sides, and keel, they require localized high levels of Q_x to force those regions to a zero radial displacement condition. Therefore, there is a slight stress resultant concentration for Q_x in the overlap regions at the cylinder ends. The circumferential transverse shear stress resultant Q_y is zero over much of both cylinders. At the overlaps, however, because of the tendency of the crown and side segments to deform outward by different amounts, there are highly localized nonzero values of Q_y in both cylinders. In fact, the peak values of Q_y are comparable to the peak values of Q_x, with the peaks occurring near the clamped ends on both sides of the overlaps.

The axial bending moment resultant M_x, the circumferential bending moment resultant M_y, and the twist moment resultant M_{xy} are zero except in the bending boundary layer and, interestingly enough, along the entire length of the overlaps. The nonzero values in the bending boundary layers are expected because they would be nonzero there for a cylinder constructed from a single laminate due to the axial bending response near the clamped end. However, the nonzero value in the overlaps results because of the eccentricity of the overlaps. Viewed differently, because the reference surface for the analysis is the midsurface of the segments, the bending–stretching coupling terms, that is, the B_{ij} terms in the laminate stiffness matrix, are nonzero for the overlaps. Therefore, an applied axial strain produces all three bending moment resultants in the overlaps, although M_x is the largest in magnitude. The eccentricity, coupled with the bending boundary layer and the slightly thicker overlaps, results in slight concentrations of the moment resultants in the overlaps at the clamped ends.

Nonlinear Prebuckling Response

In this section, the results for axially stiff and circumferentially stiff cylinders subjected to a compressive axial displacements of $\Delta/\Delta_{cr} = 0.956$ and 0.995, respectively, will be discussed. These displacement levels are close to the buckling levels, but are still in the prebuckling range. The corresponding axial loads for these two displacement levels are $P/P_{cr} = 0.975$ and 0.997, respectively. The axial displacement response for both cylinders remains linear with axial position, and there are circumferential displacements, which, like in the linear prebuckling range, are largest at midlength location of the overlaps. Figures 4c and 4d show the predicted normalized radial displacement responses for the axially stiff and circumferentially stiff cylinders in the nonlinear prebuckling range, respectively. Compared to the linear prebuckling range cases (Figs. 4a and 4b), there is a significant difference. For the axially stiff cylinder there is considerable wrinkling of the crown, whereas the sides are much less wrinkled. For the circumferentially stiff cylinder, there is considerable wrinkling of the sides, whereas the crown and keel are much less deformed. Of course, with the larger axial endshortening levels in the nonlinear prebuckling range, the radial displacements are larger than for the linear prebuckling range. Why certain segments wrinkle and others do not is a function of the portion of the axial load being reacted by each segment and the bending stiffness and arclength of the segment. For the axially stiff cylinder, for the linear prebuckling endshortening level, the crown and keel each react 29% of the total axial load, whereas the sides each react but 14%. For the circumferentially stiff case, the sides each react 28% of the total axial load and the crown and keel each react 17%.

The axial force resultant N_x for the cylinders in the nonlinear prebuckling range of response is shown in of Figs. 5c and 5d. Overall, there is not a large difference between the linear prebuckling and the nonlinear prebuckling cases for either cylinder. For each cylinder, the range of values of N_x is about the same as for the respective linear prebuckling cases. There is, however, some load redistribution in the crown of the axially stiff case due to the axial wrinkling. The same can be said for the wrinkled sides of the circumferentially stiff case. Specifically, the segment that is wrinkled sheds some of its axial load into the unwrinkled portions of the segment parallel with and near the overlaps, and also into the overlaps. The maximum value of N_x is again in the overlaps, with a slight concentration at the cylinder ends. For the segments that are not wrinkled, the value of N_y is zero, except at the clamped ends, whereas in the wrinkled segments the value of N_y varies slightly from zero in the crest and trough of the wrinkles, as well as being nonzero at the clamped ends, as was the case for the linear prebuckling range. The magnitude of these variations is small compared to N_x. The same can be said for N_{xy}, with the exception that there are slight concentrations at the ends of the cylinder in the overlap regions.

The cylinder wrinkling in the nonlinear prebuckling range causes nonzero levels of Q_x at the locations where the axial curvature changes signs. In contrast, in the linear prebuckling range of endshortening, the value of Q_x was zero over much of the cylinder. The values in the wrinked regions of the segments are close to the value of Q_x near the clamped ends to enforce the zero radial displacement condition in that segment. There are higher values of Q_x in the overlaps at the clamped ends. The peak values of Q_y are near the clamped ends, at the overlaps. The peak values of Q_y are comparable in value to, if not greater than, the peak values of Q_x.

Likewise, whereas in the linear prebuckling range the axial bending moment resultant M_x was zero over almost the entire cylinder, except at the clamped ends and, due to the eccentricity, in the overlaps, in the nonlinear prebuckling range in the wrinkled regions, the axial bending moment resultant varies in magnitude and sign. The variation in the wrinkled regions is expected because M_x, the other two moment resultants, M_y and M_{xy}, and the transverse shear force resultants, Q_x and Q_y, are all coupled through the equilibrium equations. The varying axial curvature in the wrinkled regions causes all of these related quantities to vary. The magnitude of the axial bending moment in the wrinkled region of a particular segment is the same as near the clamped end of that segment, which is much less than the value in the overlaps away from the clamped ends due to the eccentricity. In the overlaps at the clamped ends, there are concentrations of M_x. The characteristics of the circumferential and twist moment resultants are quite similar to those of M_x, but their peak values are less.

Before discussing buckling and postbuckling, note that the slight softening in the load vs endshortening relation for both cylinders in Fig. 3 just to the left of the buckling points is due to the wrinkling of the axially stiffer segments, which, in the linear range of prebuckling, react a greater percentage of the axial load than the segments that do not wrinkle. Wrinkling itself reduces the axial stiffness of the cylinder, but wrinkling also causes some of the axial load to be redistributed to the segments that are axially softer. The totality of effects is a softening of the cylinder in the axial direction when wrinkling begins.

Buckling Response

As the endshortening is increased within the prebuckling range of response, the tangent stiffness matrix associated with the finite element model of the cylinder ceases to be positive definite. In this study, this is considered the buckling condition for the cylinder. As indicated earlier, the buckling level of endshortening is Δ_{cr} and the associated load P_{cr}. The STAGS finite element code reports the absence of the positive definite condition by indicating the tangent stiffness matrix has a negative, or zero, eigenvalue. If the endshortening is greater than Δ_{cr}, the eigenvalue will be negative because the cylinder has been loaded to a statically unstable condition. The challenge is to find the value of Δ that causes the lowest eigenvalue to change sign, that is, the zero eigenvalue condition. This requires increasing and decreasing Δ by small amounts near the buckling condition until the exact condition is found. The endshortening values for the

Table 1 Normalized buckling parameters

Analysis	$\frac{\Delta_{cr}}{(\Delta_{cr})_{zero\ eig}}$	$\frac{P_{cr}}{(P_{cr})_{zero\ eig}}$
Axially stiff cylinder[a]		
Zero eigenvalue condition	1.000	1.000
Classic linear bucking analysis	0.949	0.994
Buckling analysis conducted at an endshortening level 85% of the zero eigenvalue condition	1.139	1.000
Buckling analysis conducted at an endshortening level 95% of the zero eigenvalue condition	0.986	1.008
Circumferentially stiff cylinder[b]		
Zero eigenvalue condition	1.000	1.000
Classic linear buckling analysis	0.929	0.989
Buckling analysis conducted at an endshortening level 85% of the zero eigenvalue condition	0.996	1.020
Buckling analysis conducted at an endshortening level 95% of the zero eigenvalue condition	1.018	1.031

[a] $(\Delta_{cr})_{zero\ eig} = 0.891$ mm (0.0351 in.) and $(P_{cr})_{zero\ eig} = 88{,}100$ N (19,810 lb).
[b] $(\Delta_{cr})_{zero\ eig} = 2.76$ mm (0.1087 in.) and $(P_{cr})_{zero\ eig} = 142{,}500$ N (32,000 lb).

zero eigenvalue condition for the axially stiff and circumferentially stiff cylinders are 0.891 and 2.76 mm (0.0351 and 0.1087 in.). The corresponding loads are 88,100 and 142,500 N (19,810 and 32,000 lb). These are the values used to normalize the relationships in Fig. 3. Other methods of computing the buckling conditions can be used. As a comparison, classic linear buckling analyses and buckling analyses performed at geometrically nonlinear states corresponding to endshortening to 85 and 95% of the buckling endshortening value as given by the zero eigenvalue condition were conducted. Of course the classic linear buckling analysis is conducted with the condition of no (0%) axial endshortening. Table 1 summarizes the buckling values of Δ and P computed by these various analyses. To ease the comparison, for each cylinder the values in Table 1 are normalized by the value computed for the zero eigenvalue condition for that cylinder. It is seen that for the axially stiff cylinder, the one alternative analysis gives a prediction for the buckling endshortening value that is approximately 14% higher than the zero eigenvalue condition. For the circumferentially stiff cylinder, the classic linear bucklng analysis gives a prediction 7% lower than the zero eigenvalue condition. It can be concluded that the slight nonlinearity in the load vs endshortening relations near the buckling point does not have a significant effect on the predictions. The radial displacement contours of the buckling displacements for the linear eigenvalue analysis for each cylinder look very much like the displacements from the nonlinear prebuckling analysis (Figs. 4c and 4d).

Postbuckling Response

When the endshortening is increased beyond the buckling point, the cylinder deformations depart significantly from those observed up to the point of buckling, and the axial load supported suddenly decreases. This load decrease is indicated in Fig. 3 by the drop from point A to point B. The cylinder deformations consist of large localized inward and outward radial displacements and are in contrast to the periodic wrinkling response observed in the prebuckling range of endshortening. The transition from the state just before buckling, through buckling, and to this state of large localized deformations occurs suddenly. It is a dynamic event and must be treated as such. With increased endshortening beyond point B to point C, the load level increases again. Because of the large inward and outward deformations of the postbuckled state, the overall axial stiffness decreases relative to the prebuckling values, and as a result, the slope of the load vs endshortening relation from point B to point C is considerably less than the slope in the prebuckling region of the relation. In the study, a transient dynamic approach was taken to move from point A to point B. A brief outline of the steps taken follow, assuming that the configuration of the cylinder is unstable at point A, the zero eigenvalue condition.

Step 1 is to incorporate proportional damping of the form

$$[C] = \alpha[M] + \beta[K] \tag{3}$$

into the finite element model, where α and β are mass and stiffness damping factors, respectively. The STAGS users manual[6] provides guidance on selecting numerical values for α and β for a particular problem.

Step 2 is to begin the transient dynamic solution using a numerical time integrator and, with the endshortening fixed at a level corresponding to point A, apply a small inward pressure load over a specific short time interval, that is, apply a weak inward pressure pulse. A pressure pulse from 6890 to 13,790 Pa (1 to 2 psi) in magnitude applied in a ramp-up then ramp-down fashion over a time interval of 0.001 to 0.002 s initiates the dynamic analysis. In principle, with no damping, simply initiating a dynamic analysis at statically unstable point A would be all that is necessary. However, with damping, the movement away from point A could be slow, requiring long integration times, and so the weak pressure pulse approach was adopted. (Also, it is possible that a small amount of damping would stabilize point A, and so some kind of initiator would then be necessary.) Instead of applying an impulsive inward pressure load to initiate the transient response of cylinders loaded in compression, other investigators[1] have applied an impulsive endshortening.

Step 3 is to integrate forward in time while monitoring the kinetic energy. Over time, the time-dependent behavior of the cylinder appears to be converging to a specific configuration, near point B in Fig. 3, and the kinetic energy approaches a negligible level, indicating that the transient response has attenuated. The specific configuration is considered to be similar to a stable postbuckling equilibrium configuration, and the transient analysis is terminated.

Step 4 is to use a load relaxation technique to make the transition from the dynamic analysis to the static analysis.

Step 5 is to restart the static analysis. The endshortening is slowly increased, and the path from point B to point C is found.

Note that neither the magnitude nor duration of the pressure pulse had an influence on the final outcome of the transient analysis. In another study using a pressure pulse,[8] it was also found that the direction of the pressure pulse did not influence the final outcome.

As can be seen from Fig. 3, the load drop from point A to point B for the circumferentially stiff case is quite significant. Specifically, the loads drops 57% of its buckling value. In contrast, the load drop for the axially stiff cylinder is 20% of the buckling value. The solid vertical lines from point A to point B correspond to the unstable transient buckling response of the cylinder predicted by the transient dynamic analysis. The slight continuation of the solid line downward from point B represents the dynamic overshoot as the solution converges to point B.

Figures 4e and 4f show typical postbuckling radial displacement contour plots for both cylinders. Specifically, the results for the axially stiff and circumferentially stiff cylinders correspond to endshortening levels of $\Delta/\Delta_{cr} = 1.202$ and 1.455, respectively, and this corresponds to load levels of $P/P_{cr} = 0.876$ and 0.511, respectively. As endshortening increases in the postbuckling range along path BC, the overall character of the deformation pattern remains unchanged, but the magnitude of the deformations increases. Figures 4e and 4f show clearly that for both cylinders the displacement responses are dominated by inward dimples, or localized buckles. However, the overall character of the radial deformation response is markedly different between the two cylinder constructions. In particular, the radial displacement response of the axially stiff cylinder is characterized by a single inward dimple in the crown and keel segments that is bounded by the overlap segments. In contrast, the response of the circumferentially stiff cylinder is characterized by two rows of inward dimples distributed around the circumference of the cylinder, forming an antisymmetric pattern. The two circumferential rows of dimples run along lines at $x = 3L/8$ and $5L/8$. These circumferentially aligned rows of dimples consist of six inward dimples each. The row at $x = 3L/8$ is made up of dimples that are contained in the main segments of the cylinder, two in each side segment and one each in the crown and keel segments, for a total of six dimples. The row of dimples at $x = 5L/8$ displays an alternate symmetry:

one dimple in each of the side segments and one dimple centered on each overlap, again for a total of six dimples. These two rows of dimples have as a line of antisymmetry the circumference at $x = L/2$. These two rows of dimples occurred at the same level of endshortening. This is opposed to progressive postbuckling, where some dimples formed at one level of applied endshortening, and then at an increased level of endshortening, the remaining dimples formed. For both cylinders, the dimples are separated by regions of outward displacement, which can best be characterized as ridges, in some cases rather sharp. The radial displacement pattern for the axially stiff cylinder shows that the magnitude of the radial displacements ranges from over 7 laminate thicknesses inward to just slightly under 2 laminate thicknesses outward. Similarly, for the circumferentially stiff case, the dimples are displaced over 9 laminate thicknesses inward and the ridges 3.5 laminate thicknesses outward. Overall, the axial displacements for both cylinders in the postbuckled state (not shown) vary linearly with the axial coordinate, similar to the results in the prebuckling range of endshortening. However, around the dimples there are deviations from this pattern as a result of the large inward radial displacements. Also whereas with the prebuckling level of endshortening the circumferential displacements were characterized by the overlaps moving toward the crown or keel, depending on which overlap is being considered, in the postbuckled state these motions are dominated by the large localized circumferential displacements as a result of the inward dimpling.

Note that the differences in the postbuckling radial displacement patterns of the two cylinders explains the difference in the load drops from point A to point B for the two cylinders, that is, 57% for the circumferentially stiff cylinder vs 20% for the axially stiff cylinder. Specifically, Fig. 4f shows that all segments of the circumferentially stiff cylinder participated in the postbuckling event, whereas Fig. 4e shows that for the axially stiff cylinder, only the crown and keel are involved in the postbuckling event. With all segments of the circumferentially stiff cylinders loosing axial stiffness due to dimpling, the load drop is more severe than when just the crown and keel dimple and the sides have the same axial stiffness as in prebuckling, as is the situation for the axially stiff cylinder. For the same reason, the postbuckling stiffness of the axially stiff cylinder is greater than that of the circumferentially stiff cylinder.

The stress resultants for the segmented cylinders are affected greatly by the postbuckling deformations. The axial force resultant N_x for the axially stiff cylinder in postbuckling is shown in Fig. 5e. The contour plot of Fig. 5e shows the maximum compressive value of $N_x (\approx -5.0)$ to be concentrated in the crown region of the cylinder at the edges of the dimples adjacent to the overlaps at $x = L/2$. A closer look at the stress resultant contours shows that an axial strip of the crown and keel, adjacent to and parallel with the overlaps, supports a higher level of axial stress resultant than an axial strip parallel with the overlaps but passing through the dimples. Essentially, the presence of the dimples causes the axial load in the crown and keel to be redistributed to the edges of those segments near the overlaps. The overlaps also support an increased level of stress resultant. The axial force resultant in the undimpled side segments of the cylinder is relatively uniform and considerably lower in magnitude compared to that in the overlap regions. There is an overall change in the magnitude of the axial force resultant in the postbuckling range of endshortening. Specifically, the range of normalized N_x just before buckling is from -2.39 to -0.551, whereas in postbuckling the range is from -5.07 to -0.315. For the circumferentially stiff cylinder (Fig. 5f), the axial stress resultant contour

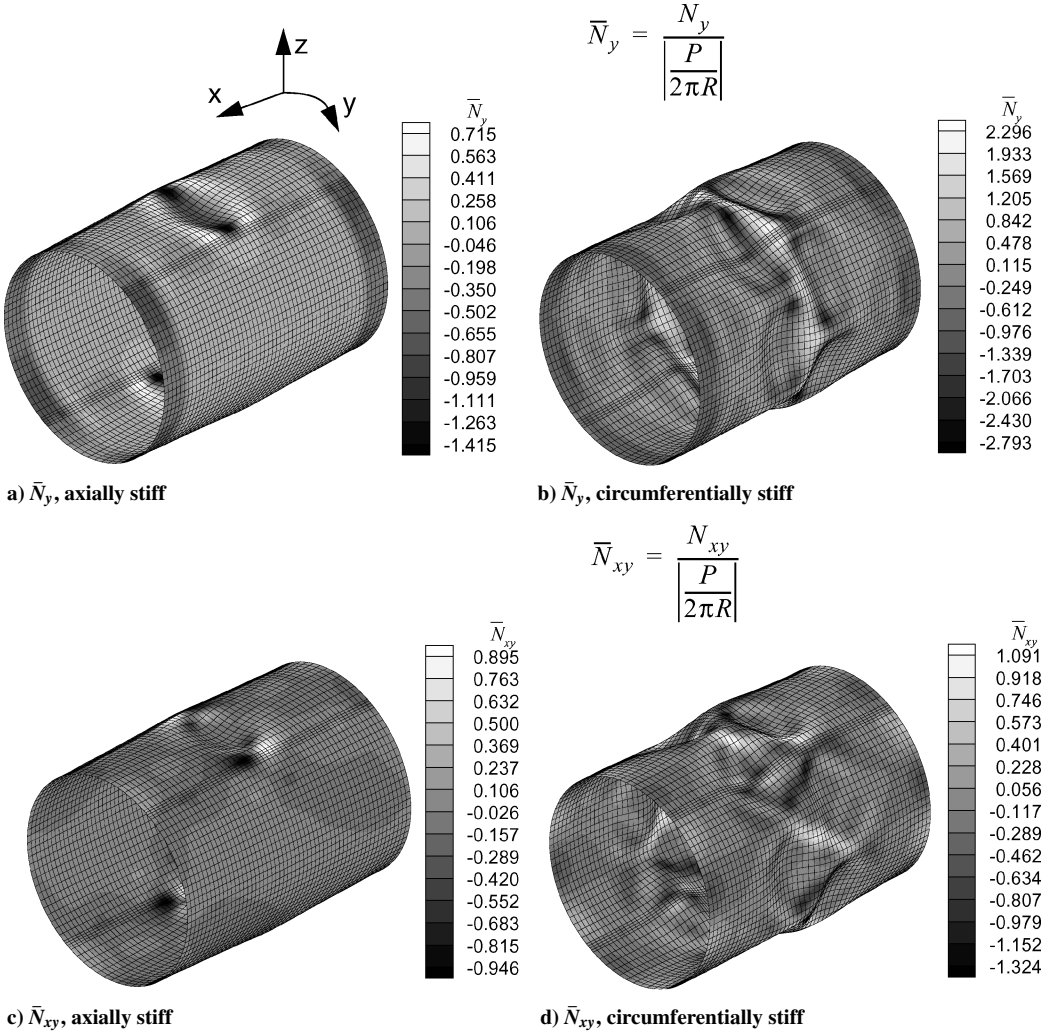

a) $\bar{N}_y$, axially stiff **b) $\bar{N}_y$, circumferentially stiff**

c) $\bar{N}_{xy}$, axially stiff **d) $\bar{N}_{xy}$, circumferentially stiff**

Fig. 6 Normalized axial force resultants, $\bar{N}_y$ and $\bar{N}_{xy}$, postbuckling.

plot shows there is a region of maximum compressive values of the axial stress resultant N_x running along the overlap from $x = 0$, toward cylinder midlength. At approximately $x = 3L/8$, the load is distributed near the ridges formed between adjacent inward dimples. This load path of high compressive N_x never reaches $x = L$; rather, the load path splits and follows the outward ridges near the overlaps between dimples at $x = 3L/8$, passes $x = L/2$ on the ridges, and then diminishes in magnitude past $x = 5L/8$ to proceed to $x = L$. The axial stress resultant is also highly compressive in the troughs of dimples that are centered on overlaps at $x = 5L/8$. The postbuckling axial stress resultant redistribution in the circumferentially stiff cylinder is illustrated by comparing the contour plot in the nonlinear prebuckling range with the corresponding prebuckling result (Fig. 5d). The prebuckling axial stress resultant is more uniform within segments and follows from the geometry and stiffness distribution of the cylinder. In postbuckling, the stress resultant is quite nonuniform, with highly localized compressive values.

As was already mentioned, for the linear and nonlinear prebuckling range for both cylinders, the value of N_y was small compared to the value of N_x. However, for the postbuckling range, shown in Figs. 6a and 6b and normalized as in Eq. (2), there are concentrated levels of N_y near the edges of the dimples. For the axially stiff cylinder, the maximum compressive values of N_y are about 28% of the maximum compressive value of N_x. For the circumferentially stiff cylinder, the maximum compressive values of N_y are over 80% of the maximum compressive value of N_x. Because, on average, N_y must be zero away from the ends of the cylinder, the regions of compressive concentrations must be accompanied by nearby regions of tension. For the axially stiff cylinder, the tension regions surround each dimple. For the circumferentially stiff case, the tension region forms a band around the cylinder at the $x = L/2$ location. The shear force resultant N_{xy} is also influenced by the presence of the dimples. For the linear and nonlinear prebuckling cases, the value of N_{xy} was zero over much of the cylinders, although there were concentrations near the cylinder ends around the overlaps. For the postbuckled configurations, N_{xy}, shown in normalized form in Figs. 6c and 6d, exhibits concentrated values associated with the dimpling that are on the order of 20% of the peak compressive value of N_x for the axially stiff case and on the order of 40% for the circumferentially stiff case. The elevated values of the three force resultants are generally in the same location and can, thus, could be the source of inplane material failure.

Contour plots of the axial transverse shear force resultants Q_x for the postbuckled configurations are shown in Figs. 7a and 7b, where the normalization of Eq. (2) has again been used. The maximum positive and negative values of Q_x in postbuckling for the axially stiff case are nearly three times the values for the nonlinear prebuckling condition, which occur in the wrinkles and at the clamped ends in the overlap. Note that for the axially stiff case, the extreme values occur within the dimples, toward their edges, near the points in the overlaps where there is a change in curvature due to the edges of the dimples meeting the overlaps. Moving in the axial direction through the dimple, the sign of Q_x changes. The contour plot of the normalized axial transverse shear force resultant shows that material failure due to interlaminar shear for the axially stiff cylinder could occur near the overlaps at $x = L/2$. For the circumferentially stiff cylinder, the values of normalized Q_x for the postbuckling response are about four times larger than the values for the nonlinear prebuckling condition. The pattern of Q_x for the circumferentially stiff cylinder shows sign changes and a degree of antisymmetry when moving

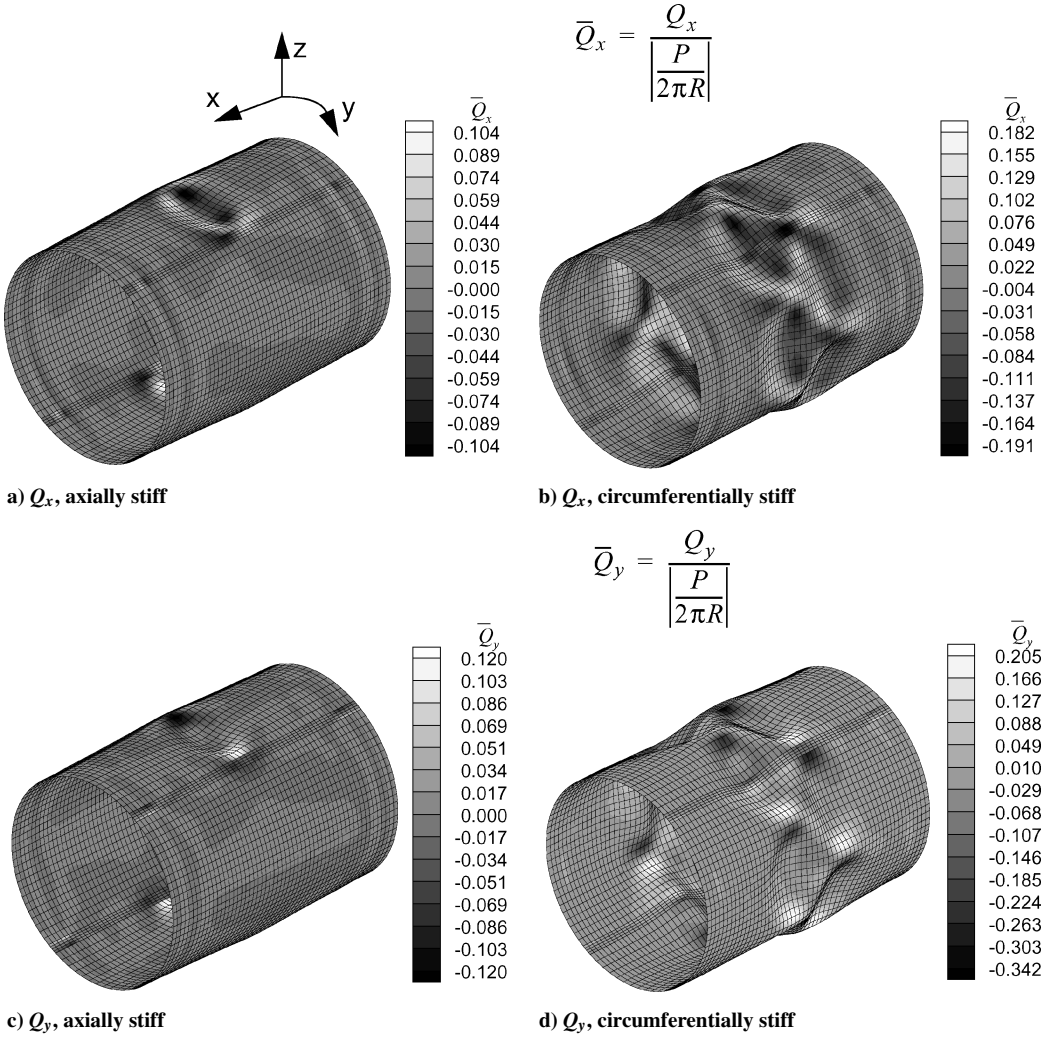

a) Q_x, axially stiff **b) Q_x, circumferentially stiff**

c) Q_y, axially stiff **d) Q_y, circumferentially stiff**

Fig. 7 Normalized transverse shear force resultants, $\bar{Q}_x$ and $\bar{Q}_y$, postbuckling.

through the dimples in the axial direction. As these patterns of antisymmetry intersect the overlaps, they lead to maximum values of Q_x in the overlaps and at the edges of the dimples. As expected, the patterns and peak values of Q_y, shown in normalized form in Figs. 7c and 7d, change considerably in the postbuckling range as compared to the prebuckling condition. The localized peak values of Q_y in the vicinity of the dimples are higher than the values of Q_x. In particular, for the circumferentially stiff case, they are almost two times higher. Some portion of the high values of Q_y are due to the geometry of the dimples, that is, at inflection points in the radial deformations, but some portions are again due to the segments and overlaps having to deform compatibly where they join, despite the differences in elastic properties.

For the axially stiff cylinder, the axial bending moment resultant M_x in the postbuckling range illustrates the one feature mentioned earlier that is also prevalent in the linear and nonlinear prebuckling ranges for both cylinders, namely, the elevated value of bending moment along the length of the overlap due to the eccentricity of the overlap. This is shown in Fig. 8a, where the values of M_x (and M_y and M_{xy} subsequently) have been normalized as

$$\bar{M}_x = M_x/[|P/2\pi R|(H/2)] \tag{4}$$

In the nonlinear prebuckling range, the values along the length of the overlaps are greater than the values in the wrinkled segments and at the clamped ends of those segments. In the postbuckled configuration of Fig. 8a, however, the values along the length of the overlaps are overshadowed by peak values at the edges of the dimples. In fact, as can be seen, the values at the edges of the dimple are similar to the values in the overlaps at the clamped ends (≈ -3.0). In the

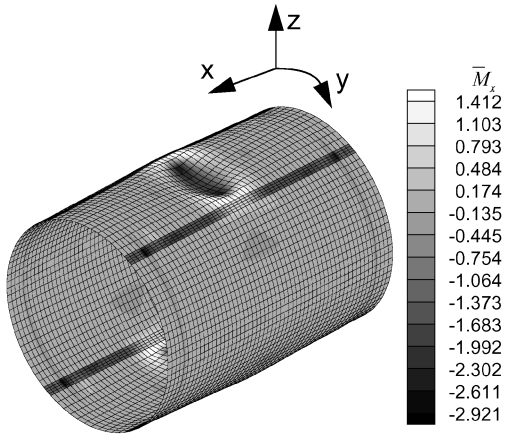

a) $\bar{M}_x$, axially stiff

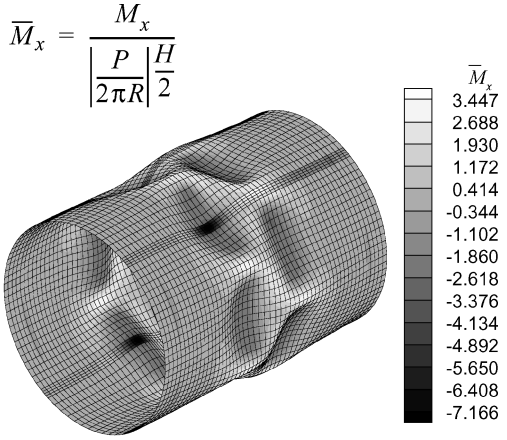

b) $\bar{M}_x$, circumferentially stiff

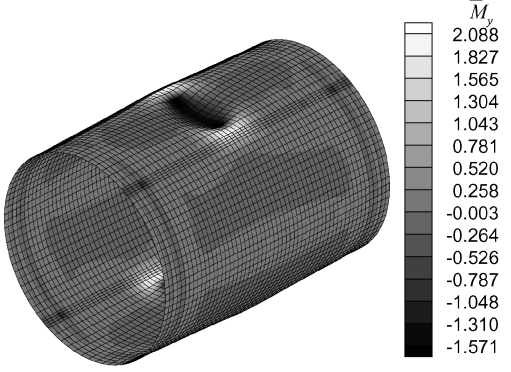

c) $\bar{M}_y$, axially stiff

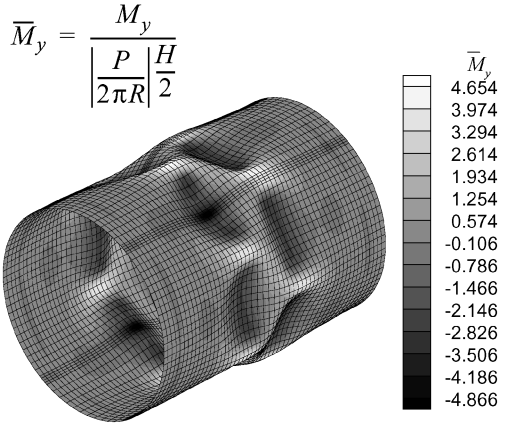

d) $\bar{M}_y$, circumferentially stiff

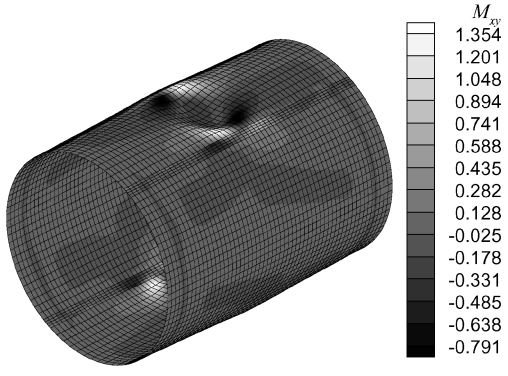

e) $\bar{M}_{xy}$, axially stiff

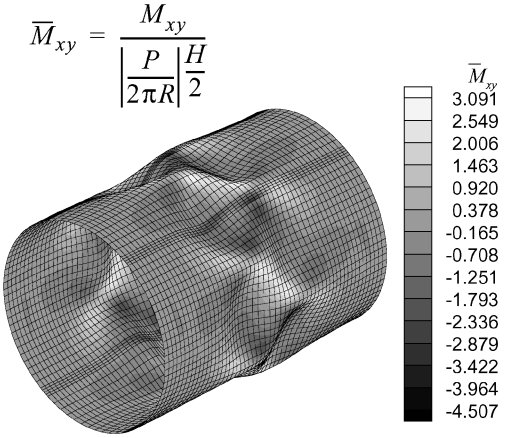

f) $\bar{M}_{xy}$, circumferentially stiff

Fig. 8 Normalized moment resultants, $\bar{M}_x$, $\bar{M}_y$, and $\bar{M}_{xy}$, postbuckling.

circumferentially stiff cylinder, Fig. 8b shows that in the postbuckling range there is a high axial bending moment at the bottom of the dimples centered on the overlaps (≈ -7.2). The value at the bottoms of the dimples overshadows any other value. For both the axially stiff and circumferentially stiff cylinders, because of the dimpling, there are high levels of circumferential bending moment resultant M_y within and near the dimples, as seen in Figs. 8c and 8d. For both cylinders, the magnitude of the peak circumferential bending moment resultant is about 70% of the magnitude of the peak axial bending moment resultant. The twist moment resultant, M_{xy}, shown in Figs. 8e and 8f, has peak values in and around the dimples. For the axially stiff case, the peak values are about 50% of the peak values of M_x, whereas for the circumferentially stiff case, the peak values are about 60% of the peak values of M_x. Like the peak values of the force resultants, the peak values of the three moment resultants are generally in the same location and, thus, could be a source of material failure.

Summary

A brief overview of the response of cylinders constructed in four circumferential segments and compressed axially has been presented. The segments were joined by slightly thicker overlap regions. Two cylinder constructions were considered. The cylinders were clamped and were compressed into the postbuckling range of response. Differences in the lamination sequence in adjacent segments led to several interesting response features. In particular, the linear prebuckling displacements were characterized by a variation of the radial displacement with circumferential position. The axial stress resultant in each segment was uniform and highly dependent on the axial stiffness of each segment. The high values of the axial transverse shear stress resultants occurred in the overlap regions at the ends of the cylinder. In the nonlinear prebuckling range, the more highly loaded segments of the cylinder began to develop wrinkles in the axial direction, whereas other segments remained wrinkle free. The stress resultants were somewhat influenced by the wrinkling, but were similar to the corresponding linear prebuckling resultants. The buckling value of endshortening for each cylinder was determined by several methods, but the agreement among the methods was good. The buckling deformations for the linear buckling analysis were similar to the nonlinear prebuckling deformations and were characterized by wrinkling in the more highly loaded segments. When loaded past buckling into the postbuckling range, the axial load dropped 57% for the circumferentially stiff construction and 20% for the axially stiff construction. The deformation pattern in the postbuckling range for both cylinders consisted of significant inward dimples, more in the circumferentially stiff cylinder than in the axially stiff cylinder, and outward displacing ridges. These dimples were on the order of 7–9 laminate thickness in amplitude inward and the ridges 2–3 laminate thicknesses in amplitude outward. This compared with radial displacements on the order of a laminate thickness or less for the linear and nonlinear prebuckling conditions. The difference in the load drop in the postbuckling range between the axially stiff and the circumferentially stiff cylinders was attributed to the fact that for the axially stiff cylinder only the crown and keel developed dimples, whereas, for the circumferentially stiff cylinder, all four segments developed dimples. With all four segments particpating in postbuckling deformations, the load drop was greater. For the same reason, the postbuckling axial stiffness for the circumferentially stiff cylinder was less than that for the axially stiff cylinder. The stress resultants developed extreme values in the inward dimples and the outward ridges, with normalized values of the stress resultants being a number of times their values in the linear and nonlinear prebuckling ranges. Because of these high values, there could be a cause for concern in regards to material failure in the postbuckling range.

Although the results presented have been for rather specific cases of two thin unstiffened cylinders, there are broader implications to the findings. First, whereas stiffeners may generally be used with thin-walled cylinders, if the relative stiffnesses of the crown, keel, and sides can be viewed as representative, then the findings here can be applied to a segmented unstiffened honeycomb cylinder with the stiffnesses distributed as discussed. For such a construction, having the lamination sequence vary circumferentially represents a very real design option. Second, it has been shown that the stiffness distribution can work in subtle ways to influence the overall response. Here the buckling load of the axially stiff cylinder was considerably lower than that of the circumferentially stiff cylinder. The low buckling resistance of the axially stiff crown and keel essentially lowered the buckling load of the entire cylinder relative to the circumferentially stiff case. In this situation, stiffness was a detriment. However, as mentioned, for the axially stiff cylinder, only the crown and keel participated in the postbuckling deformation response, and the sides were available take the load shed by the postbuckled crown and keel. This is in contrast to the circumferentially stiff cylinder, for which all four segments participated in the postbuckling deformations. As a result, the load drop for the axially stiff case was lower. In this situation, stiffness was an advantage. Of course, material failure has to be examined, and that brings up a third point. During the dynamic transition from a buckling configuration to a postbuckled configuration (more precisely, because buckling is really a very isolated situation, from a configuration just before buckling to a postbuckled configuration), the material may well fail because the stress resultants are rapidly increasing around the dimples. Therefore, the dynamic transient analysis should perhaps include a check on failure during the transition. This represents a significant computational challenge, but one that may be necessary, and one that may result in a different postbuckling response because the local softening of the cylinder due to material failure may cause a further redistribution of the load.

Acknowledgments

The work reported on herein was supported by Grant NGT-1-52112 from the Mechanics and Durability Branch of the NASA Langley Research Center to Virginia Polytechnic Institute and State University. The Virginia Space Grant Consortium and the Charles E. Minor Fellowship Program at Polytechnic Institute and State University provided additional support. The authors sincerely appreciate the financial support from all sources. The NASA Grant Monitors were James H. Starnes Jr. and Damodar Ambur.

References

[1]Hilburger, M. W., and Starnes, J. H., Jr., "Effects of Imperfections on the Buckling Response of Compression-Loaded Composite Shells," *International Journal of Non-Linear Mechanics*, Vol. 37, No. 4–5, 2002, pp. 623–643.

[2]Starnes, J. H., Jr., Hilburger, M. W., and Nemeth, M. P., "The Effect of Imperfections on the Buckling of Composite Shells," *Composite Structures: Theory and Practice*, edited by P. Grant and C. Rousseau, ASTM STP 1383, American Society for Testing and Materials, West Conshohocken, PA, 2000, pp. 529–550.

[3]Riks, E., Rankin, C. C., and Brogan, F. A., "On the Solution of Mode Jumping Phenomena in Thin-Walled Shell Structures," *Computer Methods in Applied Mechanics and Engineering*, Vol. 136, No. 1-2, 1996, pp. 59–92.

[4]Hilburger, M. W., Waas, A. M., and Starnes, J. H., Jr., "Response of Composite Shells with Cutouts to Internal Pressure and Compresson Loads," *AIAA Journal*, Vol. 37, No. 2, 1998, pp. 232–237.

[5]Knight, N. F., Jr., Rankin, C. C., and Brogan, F. A., "STAGS Computational Procedure for Progressive Failure Analysis of Laminated Composite Structures," *International Journal of Non-Linear Mechanics*, Vol. 37, No. 4–5, 2002, pp. 833–849.

[6]Rankin, C. G., Brogan, F. A., Loden, W. A., and Cabiness, H. D., "STAGS Users Manual," Advanced Technology Center, Rept. LMSC P032594, Lockheed Martin Missiles and Space Co., Inc., Palo Alto, CA, May 2001.

[7]Riddick, J. C., and Hyer, M. W., "Response of Segmented Stiffness Composite Cylinders to Axial Endshortening," *Composite Structures*, Vol. 40, No. 2, 1998, pp. 103–114.

[8]Ochinero, T. T., and Hyer, M. W., "Deformation Response of Unsymmetrically Laminated Plates Subjected to Inplane Loading," AIAA Paper 2002-1579, April 2002.

A. Palazotto
Associate Editor